Available online at www.sciencedirect.com
ScienceDirect
Progress in Natural Science 19 (2009) 321–330
Progress in Natural Science
www.elsevier.com/locate/pnsc

Local heat transfer measurements on a rotating flat blade model with a single film hole

Guoqiang Xu, Bin Yang *, Zhi Tao, Zhenming Zhao, Hongwei Wu

National Key Laboratory on Aero-Engines, School of Jet Propulsion, Beihang University, Beijing 100083, China

Received 10 March 2008; received in revised form 10 April 2008; accepted 28 May 2008

Abstract

An experimental study was performed to measure the heat transfer coefficient distributions on a flat blade model under rotating operating conditions. A steady-state thermochromic liquid crystal technique was employed to measure the surface temperature, and all the signals from the rotating reference frame were collected by the telemetering instrument via a wireless connection. Both air and CO_2 were used as coolant. Results show that the rotational effect has a significant influence on the heat transfer coefficient distributions. The profiles of h_g/h_0, which is the ratio of heat transfer coefficient with film cooling to that without film cooling, deflect towards the high-radius locations on both the pressure surface and suction surface as the rotation number (Rt) increases, and the deflective tendency is more evident on the suction surface. The variations in mainstream Reynolds number (Re_D) and blowing ratio (M) present different distributions of h_g/h_0 on the pressure and suction surfaces, respectively. Furthermore, the coolant used for CO_2 injection is prone to result in lower heat transfer coefficients.

Keywords: Film cooling; Heat transfer; Flat blade; Rotating

1. Introduction

In order to enhance the efficiency of modern gas turbine engines, the inlet temperatures of the turbine become much higher than the melting temperatures of the blade material. Therefore, several cooling methods are used on the turbine blades to ensure that they work at a safety state. Film cooling is commonly used as an effective cooling technique in gas turbine engines. In the case of film cooling, the cooling air bled from the compressor is discharged through the injection holes on turbine blades to prevent the surface from thermal loads imposed by the hot gas stream. With the aid of film cooling, a higher gas temperature at the turbine inlet is permitted, which in turn, improves the thermal efficiency of turbine engines greatly.

To better understand the physical mechanism of the film cooling process and optimize the configurations in the film hole arrangement, a considerable amount of studies have been conducted during the last four decades, and a comprehensive compilation of the available results has been encapsulated by Han et al. [1]. Usually, two parameters are used to evaluate the performance of film cooling, i.e., adiabatic effectiveness and heat transfer coefficient. However, most of the studies in the field of film cooling primarily concentrate on the determination of adiabatic effectiveness, while the heat transfer coefficient has received less attention. Actually, the determination of heat transfer coefficient with film cooling is also essential for predicting the overall thermal load on turbine blades.

In the earlier studies, Eriksen and Goldstein [2] indicated that the heat transfer coefficient with film cooling was lower than that without injection because the cooling air thickened the boundary layer. However, this conclusion

* Corresponding author. Tel.: +86 10 82339665.
E-mail address: yb1982@sjp.buaa.edu.cn (B. Yang).

1002-0071/$ - see front matter © 2008 National Natural Science Foundation of China and Chinese Academy of Sciences. Published by Elsevier Limited and Science in China Press. All rights reserved.
doi:10.1016/j.pnsc.2008.05.031

seemed only to prevail in the cases of low blowing ratios. Later, Hay et al. [3] pointed out that there was an enhancive trend of h/h_0 with the increase in blowing ratio so that a maximum value of h/h_0 reached about 1.35 for the case with an inclination angle of 35°. They deduced that the increased heat transfer coefficient was caused by the enhanced momentum exchange process between the mainstream and coolant. Andrews et al. [4] concluded that the large length-to-diameter ratios 4.85–9.92 of the film hole decreased the Nusselt number at a constant Reynolds number for 90° injection holes. With the aid of the naphthalene mass sublimation technique, Karni and Goldstein [5] studied a single row of 20° injection holes with a P/d of 5.98 on a cylinder at blowing ratios of $M = 0.5$–2.0 to determine the local heat transfer coefficient distribution.

As the importance of the heat transfer characteristics in film cooling has been realized gradually, more studies have been focused on this research area recently. Mehendale and Han [6] studied the Reynolds number effect on the heat transfer coefficient distributions on the leading edge region. Their results showed that an increase in Reynolds number increased the heat transfer coefficients. Abuaf et al. [7] measured the heat transfer coefficients for a film-cooled vane. It was found that the heat transfer coefficients on the pressure surface varied a little but showed a significant increase on the suction surface. Gritsch et al. [8] investigated the local heat transfer coefficients in the vicinity of three film-cooling holes with different hole geometries. Results showed that the significant heat transfer coefficients appeared downstream of the injection holes for expanded holes, particularly under the condition of high blowing ratios. Baldauf et al. [9] used a high-resolution IR-thermography technique to measure the local heat transfer coefficients on a flat plate surface downstream of a row of cylindrical injection holes. It was found that the local heat transfer coefficients were far from the situation without the coolant injection and were highly dependent on the specific blowing situation. Ou and Rivir [10] employed a transient liquid crystal image technique to obtain the film cooling effectiveness and heat transfer coefficient distributions on a large-scale symmetric circular leading edge with three rows of film holes. Results showed that under high turbulence conditions the film effectiveness and heat transfer coefficient increase as blowing ratio increases from 1.0 to 2.0, while further increasing the blowing ratio resulted in a reverse effect. Yu et al. [11] conducted an experimental study focusing on the effects of diffusion hole geometry on overall film cooling performance. They found that the film hole with a combined forward and lateral diffusion produced a significant increase in adiabatic effectiveness and decrease in heat transfer coefficient as compared to the straight circular hole with 30° inclination angle. Besides the highly valuable studies outlined above, Yuen and Martinez-Botas [12] performed an experimental study to measure the heat transfer coefficient (h) for single jets with streamwise angles of 30°, 60°, and 90° with a short but engine representative hole length ($L/D = 4$). The results revealed that only slight variation in h/h_0 occurred as the blowing ratio was increased with the single 30° hole, and the single 60° and 90° jets yielded a smaller heat transfer coefficient than the 30° jet. As a further study, Yuen and Martinez-Botas [13] reported the heat transfer characteristics for a row of round holes which were measured on the same experimental equipment. Recently, Wagner et al. [14] proposed a new data analysis method for transient liquid crystal measurements to obtain the adiabatic effectiveness and heat transfer coefficients. Using this method, they corrected the experimental results by taking the curvature effect into account. Yang et al. [15] studied the adiabatic effectiveness and heat transfer coefficients at various injection angles of the film hole and highly turbulent flow. They found that the inclination angle has more effect on the film cooling performance, while the turbulence intensity has more effect on the heat transfer.

Due to the great difficulty in the rotating experimental approach, only a few results about heat transfer coefficient under rotating conditions are available in the open literature. Abhari and Epstein [16] studied the time-resolved heat transfer for cooled and uncooled rotors by thin heat flux gauges. They found that the film cooling reduced the time-averaged heat transfer compared to the uncooled rotor on the blade suction surface by as much as 60%, but had relatively little effect on the pressure surface. Garg [17] used a multi-block, three-dimensional Navier–Stokes code to compute the heat transfer coefficient on the blade, hub and shroud for a rotating high-pressure turbine blade. It was found that the heat transfer coefficient was much higher on the blade tip and shroud as compared to that on the hub for both the cooled and the uncooled cases. Yang et al. [18] employed a Reynolds stress turbulence model together with a non-equilibrium wall function to calculate the film cooling effectiveness and the associated heat transfer coefficients on the leading edge of a rotating blade in a particular turbine stage. The results showed that the heat transfer coefficients increased, but film cooling effectiveness decreased with increasing rotating speed.

Although many significant results in heat transfer characteristics of film cooling have been already obtained by now, the comprehension of the heat transfer mechanism in film cooling is still quite limited, especially for the cases under rotating operating conditions. From the mechanism research's point of view, the present work aims to investigate the heat transfer characteristics on a rotating flat blade model with a single cylindrical film hole. The experimental results of detailed heat transfer coefficient distributions will be helpful to achieve a profound comprehension on the heat transfer mechanism of rotating film cooling phenomenon.

2. Experimental apparatus and procedure

2.1. Test rig

A schematic drawing of the test rig is shown in Fig. 1. It consists of a rotating test section, a telemetering data

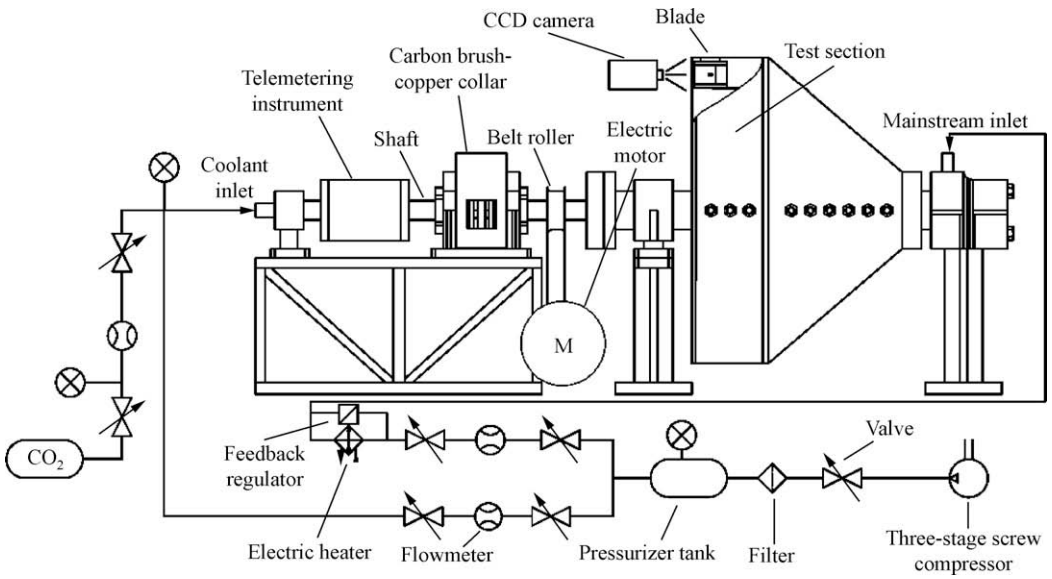

Fig. 1. Schematic view of the test rig.

acquisition system, a 30-kW electric motor for power and an air supply system. The test section is conical, and is driven by the electric motor with a maximum rotating speed of 3000 rpm. As the core component, a flat blade model is placed in the test section along the radial direction. To capture the temperature distributions on the blade surface, a high-resolution CCD camera which has a built-in flash was fixed in front of the test section without rotation. A carbon brush–copper collar device was equipped to provide the electric current for heating the test surface of the blade model. This device can switch the current from the stationary reference frame into the rotating heating sheet which adhered to the blade model. The measured temperature signals by thermocouples in the rotating test section are firstly collected and transformed into digital signals by the telemetering instrument, and then transmitted to the engineering control computer directly via the wireless connection. The air is firstly delivered by a three-stage screw compressor and transported into a pressurized tank via a filter, and then split into main and secondary flow. For both the mainstream and the coolant flow, the mass fluxes are controlled by valves and measured by flowmeters independently. Before entering the rotating test section, the mainstream is routed through a 30-kW electric heater. With the aid of a feedback regulator, the mainstream temperature can be accurately set to the desired level. In addition, a honeycombed section is placed in front of the blade model to generate a fully developed turbulent flowfield. The coolants used are air and CO_2, yielding two different averaged density ratios of $DR = 1.02$ and 1.53, respectively. For the CO_2 injection, the coolant is supplied by a steel bottle with a self-contained regulator system for temperature and pressure regulation. Through a pipe within the rotational shaft, the coolant can reach the inner plenum of the blade model directly.

2.2. Flat blade model

Fig. 2 illustrates the configuration of the flat blade model with the coordinates system employed in the current study. Due to the geometrical property of this model, the data on pressure surface and suction surface were obtained by switching the rotational direction, respectively. This model is made of bakelite which has good thermal resistance and insulativity, with a thermal conductivity of about $k = 0.28$ W/m K. The model is 142 mm long × 106 mm wide × 23 mm thick, and its front section is molding as a circular arc to lead the mainstream attaching to the wall surface closely. A cylindrical injection hole with a diameter of $D = 4$ mm is located in the middle section of the blade, and its inclination angle relative to the wall surface is 30°, giving a length-to-diameter ratio of $L/D = 5.75$. The rotational radius of this film hole is 450 mm. As seen in Fig. 2, the origin of the coordinates system is located at the downstream tip of the film hole. The x-axis is along the mainstream direction, y-axis is normal to the test surface and the z-axis conforms to the right-hand law. A composite heater plate which is 86 mm wide × 52 mm long × 3 mm thick adhered immediately downstream of the injection hole to facilitate the investigation of heat transfer coefficients. This composite heater plate is composed of two layers. The upper layer is a heating sheet that is made of a particular plastic. A carbonous slurry was sprayed homogeneously on the plastic, which can provide an even heat flux distribution. Two sheets of electric silver slurry were brushed on both the sides of the heating plate as electrodes. As the nether layer, an asbestine slate is underneath the heating sheet with a thermal conductivity of $k = 0.08$ W/m K and good thermal insulation to minimize the heat conduction through the blade model. In order to measure the temperature distributions on the

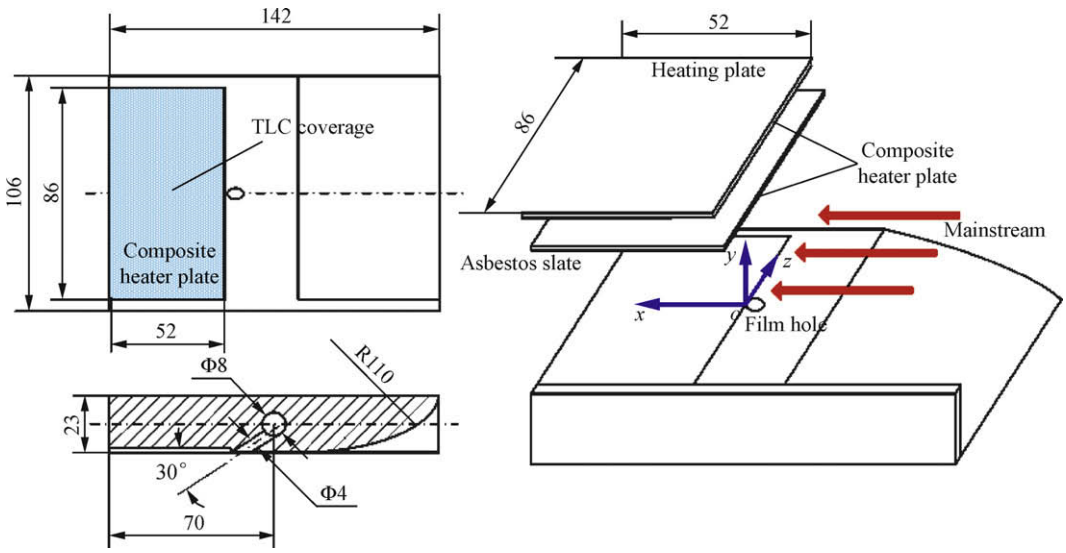

Fig. 2. Configuration of the flat blade model and coordinates system.

entire heating plate, a thin layer of wide band thermochromic liquid crystal (TLC), which had a color-changing temperature range from 30 °C to 60 °C, was sprayed onto the heating plate. Because of the inherent color of the carbonous slurry, no black paint is needed. In addition, the whole surface of the flat blade model is smooth, therefore, the mainstream flow cannot be disturbed.

2.3. Data acquisition system

Fig. 3 displays the conceptual view of the data acquisition system for the present study. A stroboscopic tachometer was used to measure the rotating speed. The mass flow rates of the mainstream and coolant were recorded, respectively, by means of an electric flowmeter and a glass rotameter. Two T-type (copper–constantan) thermocouples were located upstream of the blade model in the test section to monitor the mainstream temperature. Prior to the experiment, the thermocouples were calibrated in a constant thermal bath with a precise platinum resistance thermometer. The coolant temperature was also measured by a T-type thermocouple at the injection hole entrance of the blade chamber, and its pressure was obtained from an electric manometer. Because the hot mainstream was discharged into atmosphere directly, its pressure was assumed to be 1.01325×10^5 Pa. An additional thermocouple adhered on the backside of the test blade to monitor the temperature level and heat leakage. The temperature signals measured from thermocouples in the rotating test section were firstly collected by the telemetering instrument, and then all the signals were connected to the engineering control computer for data acquisition. The temperature distributions on the test surface were obtained by using TLC. Combined with the temperature data and TLC images, a Visual Basic program was employed to obtain the heat transfer coefficient.

2.4. Thermochromic liquid crystal calibrations

A steady-state, hue-capturing technique was adopted in the present study. To reveal the relationship between the hue value of the color image and temperature, a cal-

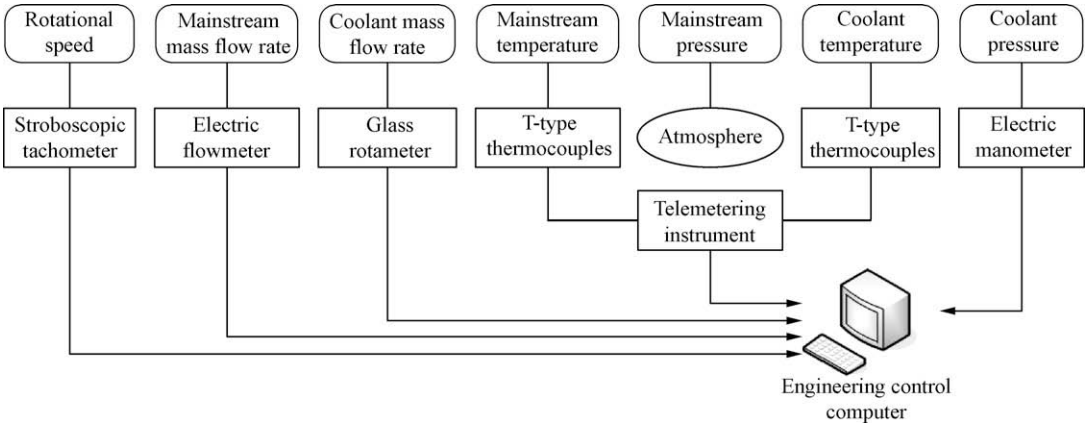

Fig. 3. Schematic of data acquisition system.

ibration experiment was performed on the test surface without injectant. The camera settings, light source, distance, and angle were kept the same for both the calibration and actual experiments. Heated by the hot mainstream, the surface temperatures were adjusted to obtain a very slow and steady temperature increase, and four calibrated K-type thermocouples with an accuracy of ±0.33 °C were mounted on the test surface to monitor the temperature. Once the surface temperature and color were stabilized, the images of the calibration were captured by the CCD camera for about each 1.5 °C temperature increase of the calibration surface from 35 °C to 60 °C and the corresponding temperatures measured by the thermocouples were recorded by an Adam4018, which had a high degree of accuracy, and were incorporated with cold junction compensation. The images captured by the CCD camera were then converted from RGB to HSI format, and the hue values were calculated averagely from the middle region of the four calibrated thermocouples. The calibration procedures were repeated three times, and the data at each time showed hardly calibration drift. By averaging the hue values at each time, a fitted polynomial curve of the hue-temperature calibration was obtained, see Fig. 4.

2.5. Evaluation criterion

The heat transfer coefficient h_g in the present study is defined as

$$h_g = q/(T_g - T_w) \tag{1}$$

where q is the wall heat flux with film cooling, T_g is the mainstream temperature and T_w is the wall temperature.

Another definition of the heat transfer coefficient h_0 is introduced

$$h_0 = q/(T_{g0} - T_{w0}) \tag{2}$$

where T_{g0} and T_{w0} are the mainstream temperature and wall temperature without film cooling. The reference case h_0 was measured in a separate experiment under the same operating conditions with that of film cooling.

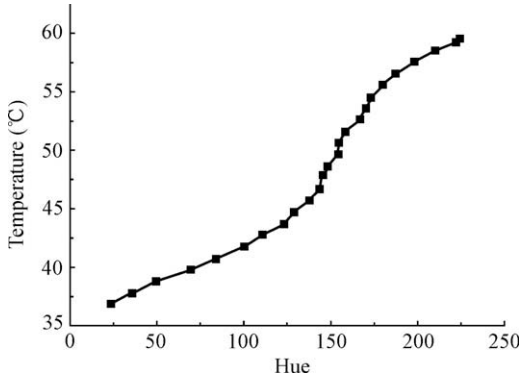

Fig. 4. Hue-temperature calibration curve for thermochromic liquid crystal.

2.6. Operating conditions and experimental uncertainties

A complete set of the operating conditions in the present study is given in Table 1.

The measured mass flow rates range from 300 kg/h to 700 kg/h for the mainstream and 0 m^3/h to 1 m^3/h for the coolant, and the rotating speed ω varies from 0 rpm to 800 rpm. The uncertainty analysis with a 95% confidence in the measured parameters is based on the method of Kline and McClintock [19]. The maximum individual uncertainties in mass flow rates for mainstream and coolant are ±20 kg/h and ±0.005 m^3/h; temperatures for mainstream and coolant are ±0.45 °C, rotating speed is ±1 rpm, and pressure for coolant is ±10 kPa. For the dimensionless heat transfer coefficient h_g/h_0, the maximum uncertainty of ±15% is estimated.

3. Results and discussion

Fig. 5 illustrates the contours of the non-dimensional heat transfer coefficient h_g/h_0 for air injection and CO_2 injection under different blowing ratio conditions. The particular cases shown here are $Re_D = 3191$ and $Rt = 0$. It can be clearly seen that the values of h_g/h_0 decrease with the increase in x/D for both air injection and CO_2 injection, and the most obvious variations in h_g/h_0 only occur in the near-hole region of $x/D < 3$ as M increases. Moreover, the maximum value of h_g/h_0 occurs in the region of $z/D = 0$–1 for various blowing ratios. This phenomenon was also observed by Yuen and Martinez-Botas [12].

To account for the lateral spreading of the cooling jet and to give a more reasonable explanation, the local heat transfer coefficients are averaged across the lateral span. Fig. 6 presents the laterally averaged distributions of heat transfer coefficient ratios h_g/h_0 versus x/D downstream of the film hole under stationary operating conditions. From Fig. 6, it can be observed that the trends of h_g/h_0 versus x/D are quite different for various values of M. At the lower blowing ratios, $M = 0.4$ for air injection and $M = 0.4$–0.8 for CO_2 injection, the trend of h_g/h_0 is to increase for the first 2D region downstream of the film hole, and then to decrease gradually with the increased streamwise distance. However, at higher blowing ratios, $M = 0.6$–2.0 for air injection and $M = 1.0$–2.0 for CO_2 injection, the values of h_g/h_0 decline continuously down-

Table 1
Definitions of dimensionless parameters and operating conditions.

Parameters	Range
Mainstream temperature (K)	327.15–329.15
Coolant temperature (K)	313.15–314.15
Reynolds number Re_D [$=\rho_0 u_0 D/\mu_0$]	1841, 3191, 4296
Rotation number Rt [$=\omega D/u_0$]	0, 0.0094, 0.0155, 0.0249
Blowing ratio M [$=(\rho_c u_c)/(\rho_0 u_0)$]	0.2–2.0
Density ratio DR [$=\rho_c/\rho_0$]	1.01–1.03 (air), 1.52–1.54 (CO_2)

Subscripts: 0 – in the absence of film cooling; c – coolant.

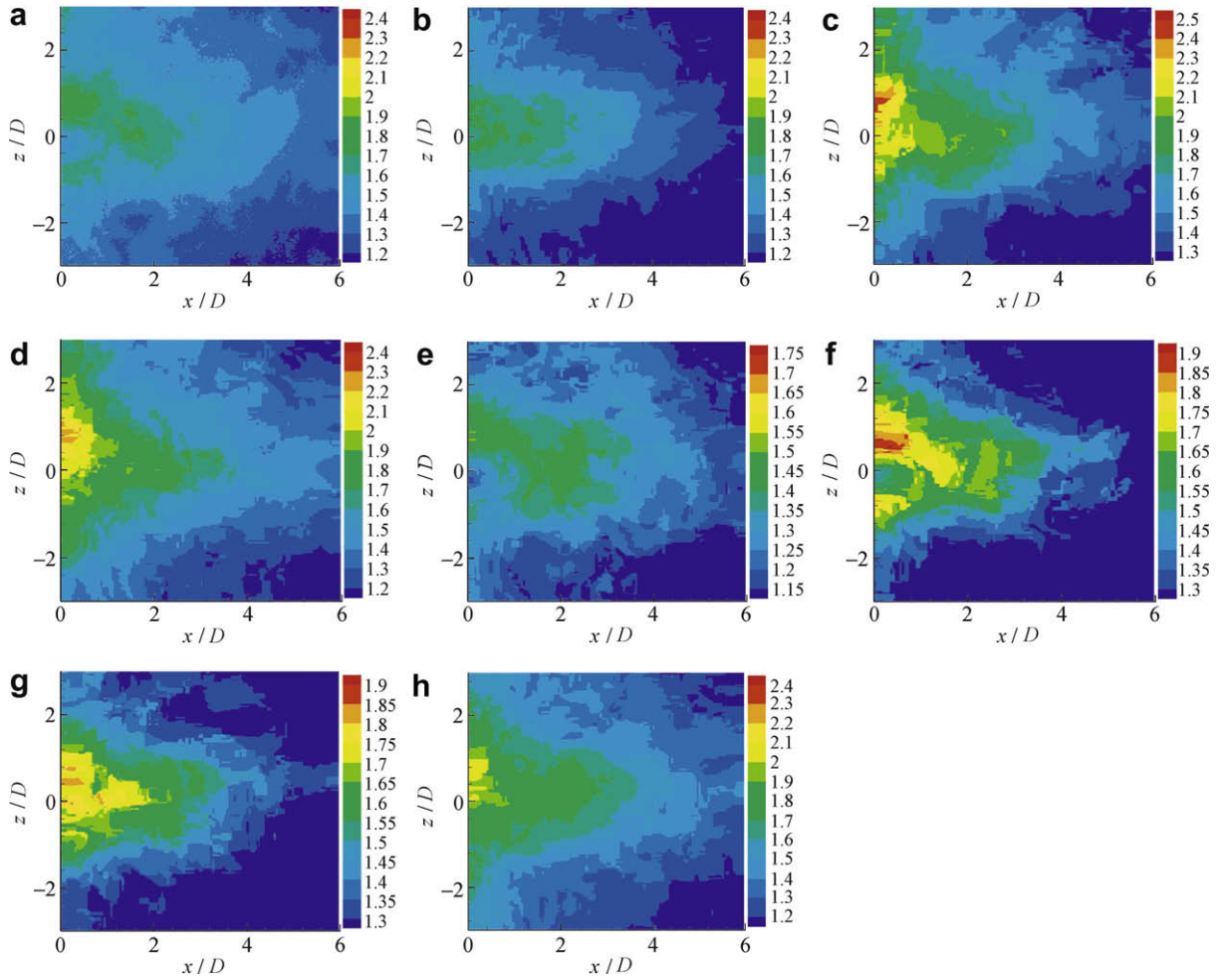

Fig. 5. Heat transfer coefficient h_g/h_0 at $Re_D = 3191$ and $Rt = 0$. (a) Air injection, $M = 0.4$; (b) air injection, $M = 0.8$; (c) air injection, $M = 1.2$; (d) air injection, $M = 1.6$; (e) CO_2 injection, $M = 0.4$; (f) CO_2 injection, $M = 0.8$; (g) CO_2 injection, $M = 1.2$; and (h) CO_2 injection, $M = 1.6$.

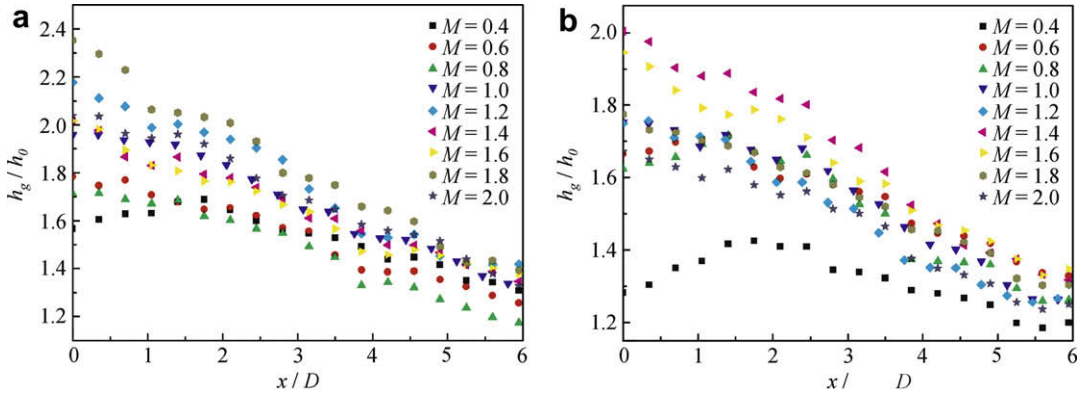

Fig. 6. Laterally averaged heat transfer coefficient h_g/h_0 at $Re_D = 3191$ and $Rt = 0$. (a) Air injection and (b) CO_2 injection.

stream of the film hole. In the near-hole region ($x/D < 4$), the variation in blowing ratio shows a strong influence on h_g/h_0, and a maximum difference by up to 35% can be observed at the tip point of the film hole. However, the variation in M only has little influence on h_g/h_0 in the far downstream region ($x/D > 4$), and the difference of laterally averaged values of h_g/h_0 is less than 8.3% as M increases from 0.4 to 2.0. In the vicinity area of the film hole, the intense turbulent mixing leads to high values of h_g/h_0 which are more sensitive to the variation in the blowing ratios. While with the development of boundary layers, the disturbance of the secondary flow onto the mainstream becomes weaker, and impairs the influence on h_g/h_0 by the variation in the blowing ratio with the increased x/D.

Fig. 7 shows the profiles of h_g/h_0 for air and CO_2 injection on the pressure surface (PS) and suction surface (SS) at $Re_D = 3191$, $Rt = 0.0249$ and $M = 0.6$. As can be observed in Fig. 7, the contours of h_g/h_0 for both air injection and CO_2 injection have deflected from the horizontal centerline of the film hole to the high-radius locations, and the deflective tendency of h_g/h_0 distributions is more evident on the suction surface. It is well known that there are three governing forces in the rotating system, i.e., the centrifugal force, Coriolis force and the buoyancy force. The buoyancy force can be negligible due to the small differential of temperature between the mainstream and coolant in the current study. The centrifugal force is prone to drive the air to high-radius locations especially for the high-density coolant flow, and this effect becomes more apparent as the angular speed increases. Differing with the action of centrifugal force, the Coriolis force pushes the cooling jets upwards and downwards along the radial direction near the suction surface and pressure surface, respectively. Therefore, due to the integrated effect of centrifugal force and Coriolis force, the coolant deflection phenomenon is more evident near the suction surface, and leads to the corresponding deflective profiles of h_g/h_0 on this side.

Fig. 8 shows the profiles of laterally averaged heat transfer coefficient h_g/h_0 along the streamwise distance at $Re_D = 3191$ and $Rt = 0.0249$. Compared with Fig. 6, it can be clearly found that the profiles of h_g/h_0 for the rotating cases are quite different from those for the stationary cases. As shown in Fig. 8(a), the trend of h_g/h_0 is to decrease continuously with the increase in x/D on the pressure surface for the air injection. The variation in blowing ratio has a moderate influence on h_g/h_0 in the entire test region ($x/D = 0$–6). While on the suction surface, the overall trend of h_g/h_0 is to decrease rapidly for the first 1D region downstream of the film hole, and then to increase gradually in the region of $x/D = 1$–3 until reaching a plateau level at $x/D = 4$–6. In addition, the influence of blowing ratio on h_g/h_0 on the suction surface is greater than that on the pressure surface due to the more intense coolant detachment. As mentioned above, the Coriolis force will weaken the centrifugal effect near the pressure surface due to its opposite direction. This leads to a different deflective angle of the film trajectory. Therefore, the values of h_g/h_0 decline sharply in the near-hole region on the suction surface. Due to the subdued interaction between the mainstream and cooling jets, the tendency of h_g/h_0 versus x/D becomes much milder in the downstream region. For the

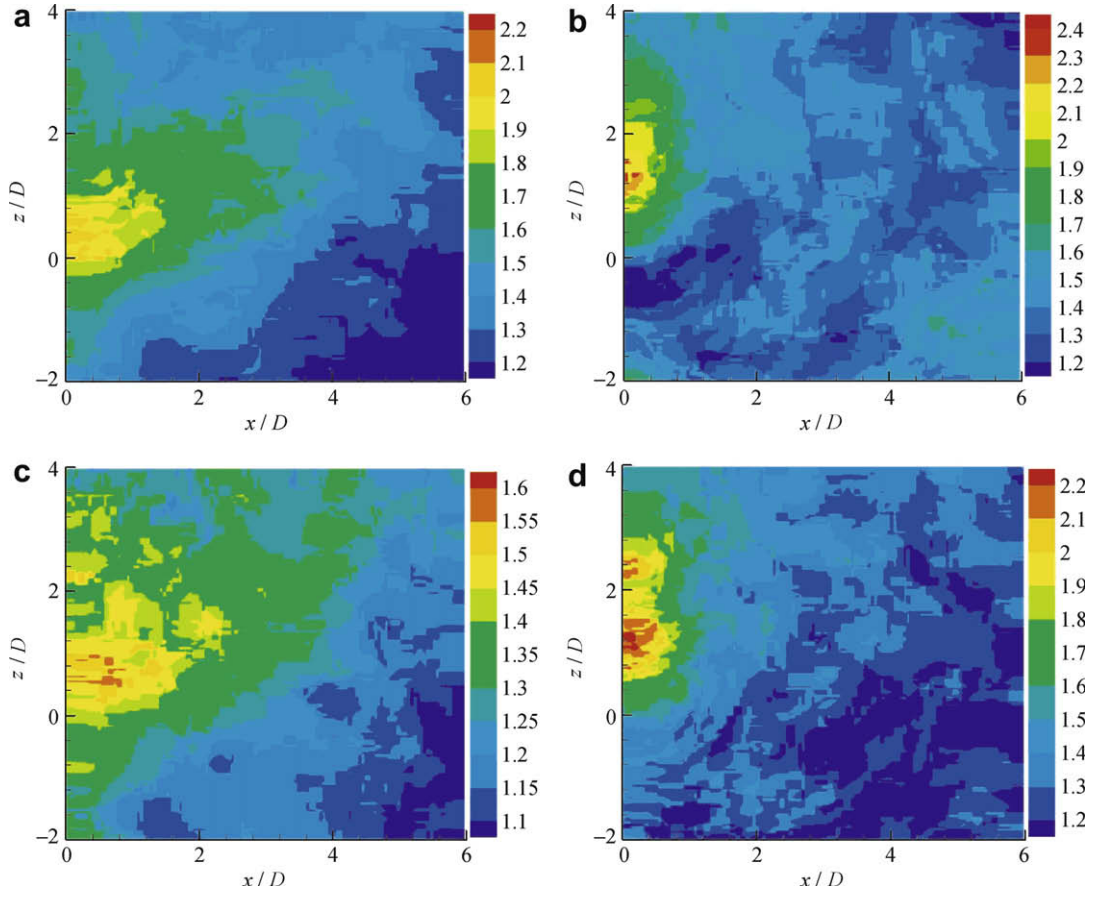

Fig. 7. Heat transfer coefficient h_g/h_0 at $Re_D = 3191$, $Rt = 0.0249$ and $M = 0.6$. (a) Air injection, PS; (b) air injection, SS; (c) CO_2 injection, PS; and (d) CO_2 injection, SS.

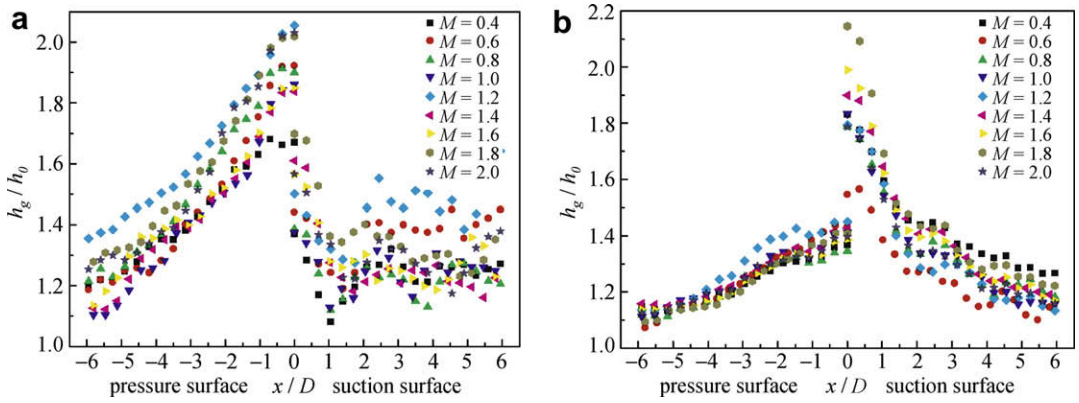

Fig. 8. Laterally averaged heat transfer coefficient h_g/h_0 at $Re_D = 3191$ and $Rt = 0.0249$. (a) Air injection and (b) CO_2 injection.

CO_2 injection, the tendency of h_g/h_0 declines continuously on both the pressure surface and suction surface, see Fig. 8(b). Meanwhile, the values of h_g/h_0 on the pressure surface are much lower than those on the suction surface especially in the region of $x/D = 1$–3. Compared with the results obtained by air injection, the overall magnitudes of h_g/h_0 on the pressure surface are much lower.

Fig. 9 illustrates the detailed heat transfer coefficient distributions for air injection in the near-field of the film hole at three values of Rt. The particular cases shown here are $Re_D = 3191$ and $M = 1.2$. As shown in Fig. 9, the profiles of h_g/h_0 have deflected towards the high-radius locations gradually on both the pressure surface and suction surface as Rt increases from 0.0094 to 0.0249, and the deflective tendency of h_g/h_0 is more evident on the suction surface. For the case of $Rt = 0.0249$ on the suction surface (see Fig. 9(f)), only a small region covered with the enhancive heat transfer appears upward of the film hole.

Compared with the cases shown in Fig. 9, the profiles of h_g/h_0 for CO_2 injection are similar for the same operating conditions. Due to the high density of CO_2 injection, the outlet velocity of cooling jets decreased at a constant value of M, and therefore the penetration of jet into mainstream can be reduced in comparison to the air injection. Therefore, the coolant used for CO_2 injection is propitious to flow closely to the wall surface, and will lead to a more uniform and improved film coverage. Furthermore, the CO_2 injection can also result in lower heat transfer coefficient ratios especially at high blowing ratios. Due to the intense turbulent mixing, the influences of air injection and CO_2 injection on h_g/h_0 have only a small difference at low blowing ratio

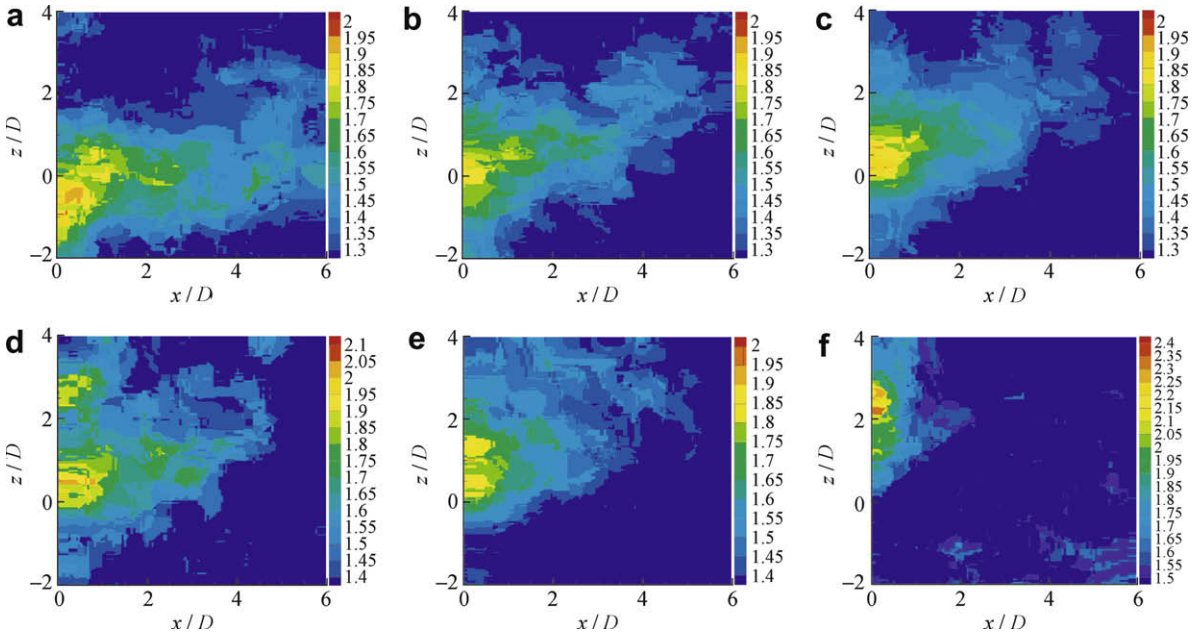

Fig. 9. Heat transfer coefficient h_g/h_0 for air injection at $Re_D = 3191$ and $M = 1.2$. (a) $Rt = 0.0094$, PS; (b) $Rt = 0.0155$, PS; (c) $Rt = 0.0249$, PS; (d) $Rt = 0.0094$, SS; (e) $Rt = 0.0155$, SS; and (f) $Rt = 0.0249$, SS.

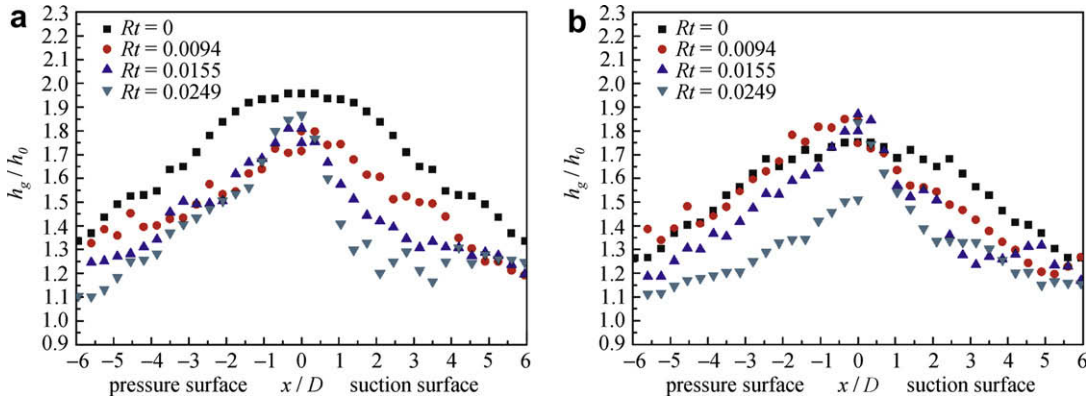

Fig. 10. Laterally averaged heat transfer coefficient h_g/h_0 at $Re_D = 3191$ and $M = 1.0$. (a) Air injection and (b) CO_2 injection.

conditions, but the distinction becomes more obvious as M increases to 2.0 (see Ammari et al. [20]).

Fig. 10 shows the laterally averaged distributions of heat transfer coefficient h_g/h_0 for air and CO_2 injection at $Re_D = 3191$ and $M = 1.0$. As seen in Fig. 10, the values of h_g/h_0 decline with x/D continuously with the streamwise development of coolant. The total range of h_g/h_0 for air injection and CO_2 injection varies from 1.1 to 2.0 approximately, and the peak values always occur in the near-hole region. As the coolant flows downstream, the enhancement of heat transfer becomes weak and is in the magnitude of 10–30% in the region of $x/D \geqslant 4$. The h_g/h_0 decreases with the increase in Rt on both the suction surface and pressure surface, and the degressive tendencies of h_g/h_0 are more evident on the suction surface. As mentioned above, this can be also attributed to the different coolant deflection phenomena beside the pressure and suction surfaces.

Fig. 11 presents the laterally averaged values of h_g/h_0 for air injection at $Rt = 0.0155$ and $M = 1.0$. In this figure, the variation in h_g/h_0 with increased Re_D shows distinct tendencies on the pressure surface and suction surface, respectively. On the pressure surface, all the values of h_g/h_0 augment with the increase in Re_D. While on the suction surface, the values of h_g/h_0 decline as Re_D increases to a value of 3191 firstly, but then augment again for a further increased Re_D of 4296. Usually, the magnitude of the heat transfer coefficient around a film hole is influenced by two leading factors. Firstly, it decreases with a thickening boundary layer induced by injection-added flow mass and linear momentum normal to the wall. The thicker boundary layer presents more heat convection resistance between the mainstream and the film-cooled surface. Secondly, the heat transfer coefficient may increase with enhanced flow shear induced by interaction between the injection and the mainstream [11]. As Re_D increases, the enhancive injection of cooling air causes an increase in the boundary layer thickness under the conditions of constant blowing ratio, and this can lead to the decrease in heat transfer behavior. When the Re_D further increases the intense turbulent mixing procedure induced by the enhanced jet–mainstream interaction will play a more important role in the flowfield. The counter-rotating vortices caused by the jets penetration lift jets off the wall surface and entrain hot gases from the surroundings to the surface, and result in subsequent more heat flux and the elevated heat transfer coefficient. In the meanwhile, similar trends of h_g/h_0 are also found for the CO_2 injection.

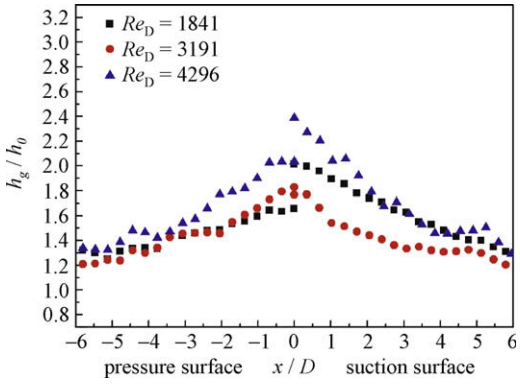

Fig. 11. Laterally averaged heat transfer coefficient h_g/h_0 for air injection at $Rt = 0.0155$ and $M = 1.0$.

4. Conclusions

Detailed distributions of local heat transfer coefficient were experimentally investigated on a flat blade model with a single cylindrical film hole under rotating operating conditions. A steady-state TLC technique was employed to measure the surface temperature, and all the signals from the rotating reference frame were collected and transmitted to the stationary receiver by the telemetering instrument. In the present study, the Reynolds number (Re_D) based on mainstream velocity and the film hole diameter varied from 1841 to 4296, the rotation number (Rt) ranged from 0 to 0.0249, and the blowing ratio (M) changed from 0.2 to 2.0. In addition, both air and CO_2 were used as coolant.

It is found that the rotational effect has a significant influence on the heat transfer coefficient distributions. The profiles of h_g/h_0 deflect towards the high-radius locations on both the pressure surface and suction surface

due to the strong centrifugal effect as Rt increases, and the deflective tendency of h_g/h_0 is more obvious on the suction surface. For the air injection, the variation in M has a moderate influence on h_g/h_0 in the entire test region on the pressure surface, while the overall trend of h_g/h_0 is to decrease rapidly for the first 1D region downstream of the film hole, and then to increase gradually in the region of $x/D = 1$–3 until reaching a plateau level. For the CO_2 injection, the tendency of h_g/h_0 declines continuously on both the pressure surface and suction surface. On the pressure surface, all the values of h_g/h_0 enhance with the increased Re_D. While on the suction surface, the distributions of h_g/h_0 decline firstly, but then augment again. Furthermore, due to the higher density, the coolant used for CO_2 injection is propitious to result in a more uniform and improved film coverage.

Acknowledgements

The work was supported by the program of New Century Excellent Talents in Beihang University (Grant No. NCET-05-0189), and was also partly funded by the Fanzhou Youth Science Foundation (Grant No. 20070401).

References

[1] Han JC, Dutta S, Ekkad SV, et al. Gas turbine heat transfer and cooling technology. New York: Taylor/Francis; 2000, p. 129–243.
[2] Eriksen VL, Goldstein RJ. Heat transfer and film cooling following injection through inclined tubes. J Heat Transfer 1974;96:239–45.
[3] Hay N, Lampard D, Saluja CL, et al. Effects of cooling films on the heat transfer coefficient on a flat plate with zero mainstream pressure gradient. J Eng Gas Turbines Power 1985;107:105–10.
[4] Andrews GE, Alikhanizadeh M, Asere AA, et al. Small diameter film cooling holes: wall convective heat transfer. J Turbomachinery 1986;108:283–9.
[5] Karni J, Goldstein RJ. Surface injection effect on mass transfer from a cylinder in crossflow: a simulation of film cooling in the leading edge region of a turbine blade. J Turbomachinery 1990;112:418–27.
[6] Mehendale AB, Han JC. Reynolds number effect on leading edge film effectiveness and heat transfer coefficient. J Heat Mass Transfer 1993;36:3723–30.
[7] Abuaf N, Bunker R, Lee CP, et al. Heat transfer and film cooling effectiveness in a linear airfoil cascade. J Turbomachinery 1997;119:302–9.
[8] Gritsch M, Schulz A, Wittig S, et al. Film-cooling holes with expanded exits: near-hole heat transfer coefficients. J Heat Fluid Flow 2000;21:146–55.
[9] Baldauf S, Schulz A, Witting S, et al. High-resolution measurements of local heat transfer coefficients from discrete hole film cooling. J Turbomachinery 2001;123:749–57.
[10] Ou S, Rivir RB. Leading edge film cooling heat transfer with high freestream turbulence using a transient liquid crystal image method. J Heat Fluid Flow 2001;22:614–23.
[11] Yu Y, Yen CH, Shih TIP, et al. Film cooling effectiveness and heat transfer coefficient distributions around diffusion shaped holes. J Heat Transfer 2002;124:820–7.
[12] Yuen CHN, Martinez-Botas RF. Film cooling characteristics of a single round hole at various streamwise angles in a crossflow. Part I: heat transfer coefficients. J Heat Mass Transfer 2003;46:237–49.
[13] Yuen CHN, Martinez-Botas RF. Film cooling characteristics of rows of round holes at various streamwise angles in a crossflow. Part II: heat transfer coefficients. J Heat Mass Transfer 2005;48:5017–35.
[14] Wagner G, Schneider E, Wolferfdorf JV, et al. Method for analysis of showerhead film cooling experiments on highly curved surfaces. Exp Therm Fluid Sci 2007;31:381–9.
[15] Yang CS, Lin CL, Gau C, et al. Film cooling performance and heat transfer over an inclined film-cooled surface at different divergent angles with respect to highly turbulent mainstream. Exp Therm Fluid Sci 2008;32:1313–21.
[16] Abhari RS, Epstein AH. An experimental study of film cooling in a rotating transonic turbine. J Turbomachinery 1994;116:63–70.
[17] Garg VK. Heat transfer on a film-cooled rotating blade. J Heat Fluid Flow 2000;21:134–45.
[18] Yang HT, Chen HC, Han JC, et al. Numerical prediction of film cooling and heat transfer on the leading edge of a rotating blade with two rows holes in a 1-1/2 turbine stage at design and off design conditions. ASME Paper, 2005; GT2005-68335.
[19] Kline SJ, McClintock FA. Describing uncertainties in single-sample experiments. Mech Eng 1953;75:3–8.
[20] Ammari HD, Hay N, Lampard D, et al. The effect of density ratio on the heat transfer coefficient from a film cooled flat plate. J Turbomachinery 1990;112:444–50.